Influence of airmass downward transport on the variability of surface ozone at Xianggelila Regional Atmosphere Background Station, Southwest China

J. Ma[1,*], W. L. Lin[1,2], X. D. Zheng[1], X. B. Xu[1], Z. Li[3], L. L. Yang[3]

1. Key Laboratory for Atmospheric Chemistry, Chinese Academy of Meteorological Sciences, Beijing 100081, China;

2. Centre for Atmosphere Watch and Services, Meteorological Observation Centre, China Meteorological Administration, Beijing 100081, China;

3. Yunnan Diqing Meteorological Bureau, Diqing 674400, China;

* Now at Atmospheric Research Center, Fok Ying Tung Graduate School, Hong Kong University of Science and Technology , Hong Kong

Correspondence to: W.L. Lin (linwl@cams.cma.gov.cn)

Abstract

In situ measurements of ozone (O_3), carbon monoxide (CO) and meteorological parameters were made from December 2007 to November 2009 at the Xianggelila Regional Atmosphere Background Station (28.006°N，99.726°E, 3580 m a.s.l.), Southwest China. It is found that both O_3 and CO peaked in spring while the valleys of O_3 and CO occurred in summer and winter, respectively. A normalized indicator (marked as 'Y') on the basis of the monthly normalized O_3, CO, and water vapor, is proposed to evaluate the occurrence of O_3 downward transport from the upper, O_3-rich atmosphere. This composite indicator has the advantage of being less influenced by the seasonal or occasional variations of individual factors. It is shown that the most frequent and effective transport occurred in winter (account to 39% of the cases on the basis of a threshold of the Y value larger than 4) and they can make a significant contribution to surface O_3 at Xianggelila. A 9.6 ppb increase (21.0%) of surface ozone is estimated based on the impact of deep downward transport events in winter. A case of strong O_3 downward transport event under the synoptic condition of a deep westerly trough is studied by the combination of the Y indicator, potential vorticity, total column ozone, and trajectory analysis. Asian Monsoon plays an important role in suppressing O_3 accumulation in summer and fall. The seasonal variation of O_3 downward transport, as suggested by the Y indicator at Xianggelila, is consistent with the seasonality of stratosphere-to-troposphere transport and the subtropical jet stream over the Tibetan Plateau.

1 Introduction

Tropospheric O_3 has been significantly increasing for more than a century due to the anthropogenic activities (Hough and Derwent, 1990; Staehelin et al., 2001; Vingarzan, 2004), deteriorating the air quality and potentially harming human beings and ecosystem (Krupa and Manning, 1988). In the troposphere, O_3 is known to be produced by gas-phase oxidation of hydrocarbons and CO under the catalysis of hydrogen oxide radicals and nitrogen oxides in the presence of sunlight (Chameides and Walker, 1973; Crutzen, 1974; Crutzen et al., 1999; Jacob, 2000). In addition to photochemical production, tropospheric O_3 also comes from the stratosphere (Junge, 1962; Danielsen, 1968). Although the chemical production is regarded as a main source of tropospheric O_3 (Fishman et al., 1979; Gidel and Shapiro, 1980), the influence of O_3 transported from the stratosphere is considerable at some background sites where the regional and local emissions of O_3 precursors are extremely limited (Ordóñez et al., 2007; Trickl et al., 2010; Logan et al., 2012; Oltmans et al., 2012; Parrish et al., 2012). Due to the stratosphere-to-troposphere exchange (STE) and the distance from the Earth surface, where sources of trace species are located, air in the upper troposphere often shows unique chemical signature. Aircraft measurements show that the climatological levels of O_3, CO, and H_2O in the upper troposphere and lower stratosphere (UTLS) over the subtropics of the Northern Hemisphere are respectively in the ranges of 80-160 ppb, 50-85 ppb, and 6-40 ppm, depending on season (Tilmes et al., 2010). Therefore, transport events of air-masses associated with stratospheric intrusions were usually characterized by high O_3, but low CO and water vapor concentrations (Marenco et al., 1998; Bonasoni et al., 2000; Stohl et al., 2000; Cooper et al., 2002; Wang et al., 2006; Langford et al., 2009; Neuman et al., 2012). Such transport events are often associated with tropopause folding synoptic systems in the middle latitudes such as cold fronts in the lower troposphere (Stohl and Trickl, 1999), corresponding with troughs/cut-off lows in the middle and upper troposphere (Davies and Schuepbach, 1994). In the mid-latitudes, the subtropical jet (STJ) stream can have significant effect on the vertical ozone distribution and the STJ varies from a wintertime maximum to a summertime minimum (Bukin et al., 2011; Koch et al., 2006). Sprenger et al. (2003) found that the downward transfer along the STJ could be even more important than the stratosphere-to-troposphere transport (STT) in the mid-latitudes and there are indications of long-range transport of high-ozone air masses that

emerged from shallow STT along the STJ (Langford et al., 1998; Langford, 1999; Koch et al., 2006; Trickl et al., 2011). Near the STJ, the occurrence frequency of double tropopauses shows a strong seasonal variation over North Hemisphere mid-latitudes, with 50–70% occurrence in profiles during winter, and a small fraction (~10%) over most of the hemisphere during summer (Randel et al., 2007), and the multiple tropopause occurrence over the Tibetan Plateau can be as high as 80% during certain winters (Chen et al., 2011). In addition, the Asian and North American monsoons may have distinct effects on the upper troposphere and lower stratosphere (Gettelman et al., 2004).

The Tibetan Plateau and the surrounding mountain range about 3,000,000 km^2 with an average elevation in excess of 4000 m a.s.l.. The kinetics and thermodynamics on the unique topography have great impact on air circulation, climate change, on local, regional or even global scales. It is important to understand the influence of transport events from the upper troposphere and the lower stratosphere, which may represent one of the most important natural input of tropospheric O_3 and impact the atmospheric radiative forcing in the Tibetan Plateau. Moore and Semple (2005) reported the existence of so called the Tibetan 'Taylor Cap' and a halo of stratospheric O_3 over the Himalaya, which causes elevated levels of the upper tropospheric O_3 along the mountain regions. This result strongly suggests that the topography of the Tibetan Plateau can exert an influence on the lower-stratosphere and upper-troposphere. Škerlak et al. (2014) compiled a global 33 yr climatology of STE from 1979 to 2011 and concluded that the Tibetan Plateau is one of the global hotpots for deep STE, where the very high orography combined with a high mixing layer enables quasi-horizontal transport into the PBL (Chen et al., 2013). So far, surface O_3 measurements in the Tibetan Plateau have been reported mainly for the Waliguan global WMO/GAW station (36.28°N, 100.90°E, 3816 m a.s.l.) in the north-eastern plateau since 1994 (Tang et al., 1995; Klausen et al., 2003; Wang et al., 2006; Xu et al., 2011) and, on the south rim, the Nepal Climate Observatory-Pyramid (NCO-P, 27.95°N, 86.80°E, 5079 m a.s.l.) in the Himalaya range (Cristofanelli et al., 2010). At Waliguan, high-O_3 events were mostly observed when transport events of the upper troposphere –lower stratosphere air occurred in spring (Ding and Wang, 2006; Zheng et al., 2011), and the summertime O_3 peak was deemed to be under the great influence of vertical mixing process including the stratosphere-troposphere exchange (Ma et al., 2002; Ma et al., 2005; Zheng et al., 2005; Liang et al., 2008) and the transport of anthropogenic pollution from central and eastern China (Xue et al., 2011). Based on the measurements at NCO-P, Cristofanelli et

al. (2010) reported an assessment of the influence of stratospheric intrusions (SI) on surface O_3 and concluded that 14.1% of analyzed days were found to be affected by SI during a 2-year investigation.

In this paper, we present 2-year (from Dec. 2007 to Nov. 2009) measurements of surface O_3 and CO at the Xianggelila station, which is located at the southeast rim of the Tibetan Plateau in Southwest China. Firstly, we give general introduction of the study including the description of observation sites, measurements of O_3 and CO, and the methods of analysis. Then, we summarize the seasonal variations of O_3 and CO, and show the main patterns of airflow which may influence the Xianggelila site. We study the impact of downward transport on surface O_3 using a normalized indicator of downward transport, which is less influenced by seasonality of trace species. In addition, we show analysis results of backward trajectories combined with the surface measurement data and demonstrate a case of O_3 transport event caused by a deep westerly trough. Finally, the influence of airmass transport from the upper O_3-rich atmosphere on the surface O_3 is assessed using the chemical tracers.

2 Measurements and methodologies

2.1 Overview of the Xianggelila station

The Xianggelila Regional Atmospheric Background Station (28.006°N, 99.726°E, 3580 m a.s.l.) is located in Yunnan province, Southwest China (Fig. 1), and is one of the background stations operated by China Meteorological Administration (CMA). The station is at the southeast rim of the Tibetan Plateau and about 450 km northwest of Kunming City (population about 7.263 millions in 2011), the capital of the Yunan province. It is considered to be weakly affected by the local anthropogenic activities because there is nearly no significant anthropogenic source of O_3 precursors surrounding the station, and the nearest township, Xianggelila County, is about 30 km away from the station. Hence，it is regarded as an ideal site for monitoring the background levels of trace gases in the atmosphere over Southwest China. The climatology of Xianggelila is mainly controlled by monsoon activities. The Asian summer monsoon can bring abundant precipitation there.

2.2 Measurements of O_3 and CO

A set of commercial instruments from Ecotech, Australia has been used to measure O_3 (9810B) and CO (9830T) at the Xianggelila station. The linearity errors for 9810B and 9830T are ±0.5% and

±1%, respectively. The lower detection limits for 9810B and 9830T are 0.4 ppb and 25 ppb, respectively. The air inlet is fixed at the height of 1.8 m above the roof of the building and about 8 m above the ground. The common inlet and all other tubing are made of Teflon. Weekly zero/span checks were done using a dynamic gas calibrator (Gascal 1100) in combination with a zero air supply (8301LC) and a set of standard reference gas mixtures (National Institute of Metrology, Beijing, China). Additional CO-free air was also produced using SOFNOCAT (514) oxidation catalysts (www.molecularproducts.com) and supplied to the CO analyzer every 2 hours for additional auto-zero (background) cycles. Multi-point calibrations of the CO analyzers were made every month. The national CO standard gas was compared against the NIST-traceable standard from Scott Specialty Gases, USA. Multi-point calibrations of the O_3 analyzer were made every month using an O_3 calibrator (TE 49i PS), which is traceable to the Standard Reference Photometer (SRP) maintained by WMO World Calibration Centre in Switzerland (EMPA). Measurement signals were recorded as 1-min averages. After the correction of data on the basis of the results of the multi-point calibrations and zero/span checks, hourly average concentrations were calculated and are used for further analysis. Meteorological data, including wind, temperature, relative humidity, etc., were also obtained from the site, with a resolution of 1 hour.

2.3 Backward-trajectory calculation and weather simulation

The HYSPLIT (Hybrid Single-Particle Lagrangian Integrated Trajectory, version 4.8) model (http://ready.arl.noaa.gov/HYSPLIT.php) was used to calculate the backward trajectories at Xianggelila from 2007 to 2009. The HYSPLIT model is a complete system for computing simple air parcel trajectories to complex dispersion and deposition simulations (Draxler and Rolph, 2003; Rolph, 2010). National Centers for Environmental Prediction (NCEP, 1° × 1°) reanalysis meteorological data were inputted for model calculation. The vertical motion method in the calculations is the default model selection, which uses the meteorological model's vertical velocity fields and is terrain following. The height of the endpoint is set at 500 m above ground level. The 3-day backward trajectories were calculated at four times (0, 6, 12, 18 UTC) per day. After calculation, the trajectories were clustered into several types using the HYSPLIT software. Besides, HYSPLIT is also used to calculate 7-day backward trajectories in a case study described in Section 3.3.

The Weather Research and Forecasting (WRF) Model Version 3.4.1 (Skamarock et al., 2005) is used to simulate the weather situations in Section 3.3 for a case study. Only one domain was initialized by NCEP FNL (Final) Operational Global Analysis data on 1.0×1.0 degree grids prepared operationally every six hours, and the space resolution of WRF is set to 36 km. The run time of WRF was set as two days and used default physical schemes.

2.4 Normalized indicator of O_3 downward transport

It is known that some species like O_3 and Be-7 are relatively high, while others like CO and water vapor are relatively low in the upper troposphere and stratosphere. Therefore, if airmasses originating from a higher elevation, for example, from the free troposphere or higher, often contain more abundant O_3, but less CO and water vapor. Cristofanelli et al. (2009) proposed a stratospheric intrusion index using baseline measurements of O_3, Be-7 and relative humidity. Such index can be used to quantify the impacts of stratospheric intrusion on ground measurements. However, long-term measurements of Be-7 are available only from few sites. Here, we try to infer whether the surface O_3 is affected by transport events from upper O_3-rich atmosphere or not according to the surface observed O_3, CO and water data. These data are available from our site and many other sites. However, the levels of O_3, CO and water vapor in the UTLS region show seasonal variations (Tilmes et al., 2010), so do their surface levels. This may make the results from different seasons less comparable. To minimize the effects of seasonal variations, we propose a normalized indicator of downward transport. For a certain period such as a month, a quantity Y, which combines the measured data of the chemical tracers of O_3, CO, and water vapor, is determined as Eq. (1).

$$Y = \frac{[O_3]}{[r][CO]} \quad (1)$$

where, $[O_3]$, [CO] and [r] denote the monthly normalized O_3, CO and water vapor mixing ratios, respectively. For example, $[O_3]$ is an hourly averaged O_3 concentration divided by the monthly averaged O_3 concentration. As Y is a composite indicator, it should be less subject to occasional disturbance in any of individual factors. Water vapor mixing ratio is calculated using the local meteorological observational data and normalized in the same way. Here, the Y indicator is used to indicate the synthesized fluctuation of O_3, CO and water vapor, which acts as a surface chemical tracer to understand the exchange of surface air with the free or upper atmosphere. The conserved

179 physical process of downward transport is assumed by the Y indicator, and this is inevitably
180 influenced by the photochemical processes of O_3 and CO. Under situations when the physical
181 processes are much more dominant than the local photochemical production in sources of surface O_3,
182 the Y indicator is expected to act as a good tracer.

183 **3 Results and discussion**

184 **3.1 Seasonal and diurnal variations of O_3 and CO**

185 The monthly averaged O_3 and CO are shown in Table 1. Both O_3 and CO reached maxima in
186 spring (O_3: 55.2±9.3 ppb, CO: 183±57 ppb), and the highest monthly-averaged O_3 concentrations of
187 58.3 ppb appeared in April. The spring maximum of O_3 at Xianggelila is consistent with the
188 observations at background sites elsewhere in the Northern Hemisphere (Monks et al., 2000). In
189 winter, the concentration of CO is low with an average level of 137 ppb, but the concentration of O_3
190 is still relatively high with an average level of 45.8 ppb. On the contrary, in summer and fall, O_3
191 level is low (29.5 ppb and 33.0 ppb, respectively), but CO remains relatively high level (152 ppb and
192 134 ppb, respectively).

193 Table 1 also shows the maxima and minima of the average diurnal variation of O_3 in different
194 months. The average diurnal variation of O_3 at Xianggelila maximizes in the early afternoon
195 (1200-1400 local time) and minimizes in the early morning. This diurnal ozone pattern seems very
196 similar with the typical diurnal O_3 pattern in urban or polluted area, where photochemically
197 produced O_3 can accumulate starting in the late morning. However, at Xianggelila, the peak O_3 at
198 daytime is strongly associated with the wind speed, as showed in Fig. 2. In the early morning, the O_3
199 mixing ratios increase sharply with the increasing wind speed. During the high-wind-speed period
200 (1200-1600 local time), O_3 maintains high levels, and then, until the beginning of the night, O_3
201 decreases with the decrease of wind speed when the turbulent downward mixing from a reservoir
202 diminishes and deposition becomes more important. Strong wind is not conducive to the
203 accumulation of the local photochemical production of O_3 and it also can force O_3 losses by
204 processes like deposition. Therefore, the transport and deposition will be the key factors than local
205 photochemical process influencing the diurnal variations of surface O_3 at Xianggelila, a remote and
206 clean site.

207 The amplitude of the diurnal variation of O_3 varies as a function of the season. The maximal
208 amplitude was found in spring, and the minimal in winter. In spring, the average daytime level of

CO is the highest among four seasons. A positive correlation between O_3 and CO (slope: 0.154, P<0.0001) during the daytime (10:00~18:00) in spring can be derived using the reduced-major-axis regression technique. Such positive O_3-CO correlation suggests photochemical production of O_3 from anthropogenic sources. This indicates the importance of photochemical origin of the spring peak. In the monsoon season, the lowest diurnal amplitude was found in August (14.5 ppb, smaller than that in June, July, and September). In August, the precipitation and cloud coverage reached the annual maximum and the mixing layer height reached the minimum (Fig. 3). The boundary mixing layer height is calculated using the surface meteorological data according to the method proposed by Cheng et al. (2001). The cloud may decrease the solar radiation and weaken the mixing ability between free atmosphere and surface. The precipitation can remove more O_3 and its precursors from the troposphere. These factors together contribute significantly to the low level of the average surface O_3 and the smaller diurnal amplitude of O_3 in monsoon season, especially in August.

3.2 Trajectory and surface measurements

3-day airmass backward trajectories during the measurement period were calculated for every 6 hours, and then grouped into 7 clusters according to their spatial similarity. The mean trajectory for each cluster, their fractions (the number of trajectories in each cluster to the total number of the trajectories), and their patterns are shown in Fig. 4. The average temperature, water vapor, O_3, and CO corresponding to each type of cluster are listed in Table 2. The dominant clusters are type 6 (55.1 %), type 5 (28.1 %) and type 7 (7.3 %), with low level trajectory heights and relatively high CO level over 135 ppb. Types 5-7 can be recognized as relatively polluted clusters. O_3 in types 6 and 7 is lowest, because these types of trajectories occur mainly in summer and fall, when Xianggelila is influenced by monsoon and abundant precipitation, which inhibit the photochemical accumulation of O_3. O_3 in type 5 is 44.8 ppb, a relatively high level and this type of trajectories mostly occur in spring and winter with less rains. Trajectories of types 1-4 are with high transport height and low CO, so they can be recognized as cleaner types in terms of CO. However, O_3 in types 1-4 is relatively high, indicating that these types of trajectories possibly carry O_3-rich airmass from the free troposphere to the surface. Types 1-4 mainly occur in winter, spring and fall, and very rare in summer.

Fig 5 shows kernel density of trajectory pressure level (the minimal one during 72-h backward trajectories), trajectory height (the maximal one during 72-h backward trajectories) and hourly Y indicator. In summer, trajectories are most likely to travel very low with high pressure levels, and smallest Y indicators are observed. The spring kernel density of trajectory resembles that in fall, but the Y indicator in spring has lower probability in the range of Y value between 3 and 7 than that in fall. This reflects that the Y indicator is able to indicate the different behavior of O_3 in different season. It is intriguing that the kernel density of trajectories in winter has a peak between 200 and 500 hPa, and accordingly, the density of Y indicator is much higher in winter than in other seasons. This is consistent with the seasonality of stratosphere-to-troposphere transport (Sprenger and Wernli, 2003; Sprenger et al., 2003) and the subtropical jet events (Koch et al., 2006) in the Northern Hemisphere. The results from Sprenger et al. (2003) demonstrate that during winter, the frequency of shallow tropopause folds is highest above the Tibetan Plateau (see Fig. 3 in their paper). Škerlak et al. (2014) concluded that, as one of the clear hotspots of deep STT fluxes into the continental PBL, there are also intense deep STT fluxes over the Tibetan Plateau during the whole year, with a peak in winter. On the basis of the intensive radiosonde observations, Chen et al. (2011) concluded that the multiple tropopause, which is associated with tropopause folds near the subtropical westerly jet, occurs in winter with a high frequency over the Tibetan Plateau, and as a result, the intrusion of air masses from the stratosphere may contribute to a higher upper tropospheric O_3 concentration in winter than in summer above the plateau. The high probability of low trajectory pressure level and the high Y value in winter implies the high probability of the occurrence of ozone downward transport in winter. In spring and fall, small peaks of the kernel density of trajectory pressure level and height are also obvious around the low pressure level at about 200 hPa to 400 hPa (1000 to 3000 m a.g.l.), but the probability is much lower than that in winter. What is intriguing is that the probability of low trajectory pressure levels and high heights is a little higher in spring than in fall, but the occurrence of a large Y indicator is higher in fall than in spring. This reverse behavior of trajectory and the Y indicator in spring and fall might imply that airmass transport from high altitudes does not necessarily enhance the O_3 level and its variation, especially in spring when photochemical production might be a significant source of O_3. It is interesting to see that there is a winter maximum around the UTLS region in the pressure panel of Fig. 5, but no maximum in the height panel. The actual reason for this is clear. The pressure levels are more comparable than the

heights because the latter are terrain-following and given in m above ground level. It should be noted that there exists a tiny peak in the kernel probability density at pressures around 430 hPa, height around 4800 m and the Y indicator around 8 in summer. This is due to a strong ozone transport event and will be discussed in Sect. 3.3.

Figure 6 shows the trajectory pressure level (or height a.g.l.) and the Y indicator in each month with their correlation coefficients and significance levels (P values). The seasonal variation of Y indicator shows a maximum in winter (2.5 to 3.0), a slight downward trend from spring to fall (1.5 to 2.0), and reached the lowest level (<1.5) in August. The trend of trajectory height is similar to that of Y indicator, while the trajectory pressure level shows an inverse trend. Relationships between trajectory pressure (and height) and the Y indicator are significant in January-June, September, November and December. The largest correlation coefficient (over 0.6) is found in March. In other months, the correlation kept around 0.2 to 0.4. Only in July, August and October the correlation is not significant, especially in terms of the relationship between trajectory height and Y indicator. The differences in significance of correlations between the trajectories and the Y indicator in the different months indicate the different contributions of the high-level airmass to surface air, resulting in the fluctuation of surface O_3, CO and water vapor. The airmass advections from the upper atmosphere might contribute significantly to surface O_3 in winter and spring. In terms of trajectory types, spring can be considered as the transition season with the origins of the trajectories changing from the Tibetan Plateau with high trajectory heights to the southwest and south of Xianggelila with low trajectory heights. The low Y indicator, trajectory height and the relationship between them in summer indicate that the factor mainly influencing surface O_3 is not regional transport, but monsoon with abundant clouds and rain as discussed in Sect. 3.1. However, there may be exceptions for some shorter periods, as shown in the next section.

3.3 A case of strong O_3 downward transport

In order to demonstrate that the Y indicator can be used to reveal the events of O_3 transport, here, we present a case with a large Y value during July 6-7, 2008. In this case, the Y value reached 43.1 in the afternoon on July 6, 2008, and this is also the largest Y value during the two years' observation. As shown in Fig. 7, surface O_3 reached a peak value of 82.4 ppb in the afternoon on July 6, 2008. At the same time, a sharp decrease of water vapor was observed.

297 Around the peak time of O_3 at 13:00, CO also showed a low level close to the detection limit (25 ppb)
298 of the CO analyzer.

299 Figure 8 shows the 7-day backward trajectories initiated at 00:00 UTC each day during the
300 period of July 4-9, 2008. On July 4, it is obvious that the air flows to Xianggelila originated from the
301 southwest with slow speed and low height (near the surface). However, the airflow path changed
302 largely from the southwest to the northwest on July 5 and kept the features till July 8, especially for
303 the airflow in the higher layer (see trajectories for the endpoint height above 1200m). During this
304 period, the airmasses in the higher layer originated from relatively high elevations (from 6000 to
305 10000 m a.g.l.), which are indicative of the lower stratosphere, travelled very fast across the north
306 part of the Tibetan Plateau and reached the surface of Xianggelila. After July 8, the origin of
307 airmasses changed back to south/southwest, similar to that on July 4. The airflow in the lower layer
308 was also influenced by local airmass during July 6-7. The co-effect by airmasses of different origins
309 in different air layers might shorten the lasting period of high surface ozone level and often cause
310 difficulty in identifying an event of O_3 transport. The Y indicator seems to be a good indicator that
311 can be further proved by the following evidence.

312 From July 5 to July 8, a deep westerly trough developed to the east and northeast of Xianggelila
313 (Fig. 9). This westerly trough began to impact Xianggelila on July 5 and extended southwesterly till
314 July 6, then retreated and diminished. The change of potential vorticity (PV) can be used to indicate
315 a strong stratospheric air intrusion into the troposphere across the tropopause. As shown in Fig. 9, a
316 high PV tongue with a large gradient along the 2 PVU (potential vorticity unit) line propagated
317 southwesterly, which indicates a strong stratospheric air intrusion into the troposphere.

318 If O_3 is strongly transported downward from the stratosphere to the troposphere, the total
319 column ozone (TCO) would temporarily increase (Vaughan and Price, 1991).When the O_3-rich air
320 intruded into the troposphere, it changed the vertical distribution of O_3 and caused a good correlation
321 between the gradient of TCO (Fig. 10) and the gradient of PV (Fig. 9). In this case, the gradient of
322 PV began to increase on July 6 when the TCO tongue appeared. The TCO value near Xianggelila
323 (red star in Fig. 10) on July 5 is around 270 DU, and it began to increase on July 6 and reached 290
324 DU on July 8 and 9. This increase is attributed to the evolution of the high TCO tongue. Together
325 with downward trajectories in Fig. 8, this event shows that the deep westerly trough brought down
326 the O_3-rich air with less water vapor and CO into the troposphere and influenced the surface.

3.4 Estimation of the frequency of O_3 downward transport

As discussed in Sect. 3.3, the Y indicator can be used to indicate the effects of O_3 downward transport. A transport event might last at a high-lying surface site for several or dozens of hours. So, if Y indicator keeps at a relatively high level for several consecutive hours or days, there may be a high possibility of an intrusion event.

There are totally 784 hours with Y higher than 3, and the times of consecutive day with Y higher than 3, 4, and 5 are 200, 136, and 91, respectively, as shown in Table 3. The numbers of consecutive days with Y higher than 8 are 15 in winter, 12 in fall, 4 in spring and summer, indicating that the Y value-deduced occurrence of transport events varies largely from season to season. The downward transport occurred most frequently in winter, followed in fall, spring and the least in summer. The seasonal cycle of our Y indicator (see Table 3 and Fig. 6) resembles that of the SI frequency at Mt. Cimone obtained by Cristofanelli et al. (2009) using a stratospheric intrusion index. Both indicators reveal that the downward transport of upper air is strongest in winter and weakest in summer. To analyze further the frequency of the downward transport, the relationship between the trajectory pressure level and Y is analyzed. The numbers of hours with both Y higher than a given value and trajectory pressure level lower than a given level are calculated for each season and shown in Fig. 11. In summer, hours with both low trajectory pressure levels and high Y values were rare, and this coincides with to the minimal O_3 mixing ratio in summer. In summer monsoon season, there were about 68.7% of days with precipitation at Xianggelila, which inhibits the accumulation of O_3. The average trajectory height (only averaged maximal height during 72 h) in summer was extremely low (134 m ending at 500 m a.g.l.), which limited the exchange of surface air with the upper free troposphere. In winter, the number of hours with both Y higher than 2 and trajectory pressure level lower than 500 hPa is nearly 2400 hours. The pressures covered by the trajectories in winter was significantly lower, indicating relatively higher O_3 from upper atmosphere to contribute the surface O_3 budget (Lefohn et al., 2001). The possibility of O_3 transport events in fall was also high with a wide range of trajectory over 1000 m and Y over 3. Together with Table 2, it is evident that the possible occurrences of O_3-rich transport events were prevailing in winter and then in fall or spring, but rare in summer.

356 Corresponding to the different frequency of the transport events in four seasons, the responses
357 of surface O_3, CO and water vapor for different trajectory pressure levels and the Y indicator are
358 examined. O_3, CO and water vapor are averaged according to the result of Fig. 11. As shown in Fig.
359 12, the trends of surface O_3, CO and water vapor respond to the distribution patterns of the trajectory
360 pressure level and Y values in spring, fall and winter. The discriminable increase of O_3 and the
361 decrease of CO and water vapor can be found with the decrease of trajectory pressure level and the
362 increase of the Y indicator except in summer. Interestingly, the trend of CO in fall is similar with
363 that in winter, but O_3 does not show significant change with the variation of trajectory pressure level
364 or the Y indicator. Because there is still monsoon influence in fall, even higher frequency of
365 transport cannot bring about a higher surface O_3, possibly due to O_3 destruction in continental stratus
366 clouds (Wang and Sassen, 2000). This reflects that the dominant factor impacting O_3 is monsoon in
367 fall. The monsoon impacts on decreasing O_3 are also reported in India (Naja and Lal, 1996; Jain et
368 al., 2005) and Eastern China and the west Pacific region (e.g., He et al., 2008). From the correlation
369 between the surface measurement and the trajectory height, as well as the Y value, it is credible that
370 the averaged surface O_3 will increase when a transport event happened with a feature of low
371 trajectory pressure level and high Y value, especially in winter. An increase of O_3 caused by deep
372 transport event is estimated as 21.0% (+9.6 ppb) in winter, by subtracting the winter average ozone
373 level (45.8 ppb) from the average O_3 mixing ratio (55.4 ppb) in the period with both trajectories
374 pressure level lower than 400 hPa and Y over 8. This is somewhat lower than the estimation of O_3
375 increase (27.1%, +13 ppb) due to stratospheric intrusions over NCO-P (Cristofanelli et al., 2010). In
376 winter, the photochemical production of O_3 is thought to be lowest. However, the winter level of O_3
377 average is 45.8±7.1 ppb at the Xianggelila station, second only to that in spring. Therefore, the most
378 occurrences of O_3 downward transport in winter may be an important reason for the higher winter
379 level of surface O_3 at Xianggelila.

380 Although the Y indicator can be used to study the influence of transport from the upper O_3-rich
381 atmosphere and obtain qualitative or semi-quantitative results, there are still open questions such as
382 what is the criterion of the Y indicator to indicate what a height for transport. Table 4 shows the
383 monthly results of the O_3–CO correlations, derived from 1000–1800 (local time) measurements from
384 Xianggelila. The correlations are statistically significant from February to November. Relatively
385 steep negative slopes are found in May, June, September, October, November and a flatter negative

slope in December, suggesting that there are clear influences from the upper troposphere and lower stratospheric air masses in these months. Significant positive O_3–CO correlations with steeper slopes are found in July, August, February, March and April, which indicate that the influences of photochemical production of O_3 are probably more important in these months.

4 Conclusions

A two-year measurement of surface O_3 and CO was made from December 2007 to November 2009 at Xianggelila in Southwest China. The maximal O_3 and CO mixing ratios were observed in spring, followed in winter and fall, and the minima was in summer. According to the analysis of backward trajectories, Xianggelila was influenced largely by the high and fast airflows from the south or north Tibet-Plateau in winter, fall and spring. In summer, trajectories to Xianggelila were mainly from the south and east regions, and their moving heights were very low under the influence of Asian Monsoon from the end of May to the end of September. As a result, the minimal O_3 was found in summer due to the most frequent precipitation and cloudiness, and the CO level in summer kept at a relatively high level because of the air transport from the south and east regions with intense anthropogenic CO emissions. The CO level was low in winter because of the airmasses originated partly from the relatively clean Tibetan Plateau.

A downard transport indicator (Y), which combined the measured data of the chemical tracers of O_3, CO, and water vapor is proposed to indicate the fluctuation of O_3 and sources from O_3-rich free troposphere. By using monthly normalized values in the calculation of Y, influences from the seasonality in the concentrations of tracers are minimized, so that the results from different seasons can be compared. A strong transport event is revealed by the largest Y indicator (43.1) during two years' observation and discussed using trajectory and weather analysis. The event was associated with a strong westerly trough and resulted in enhance of surface O_3. Together with the trajectory pressure level, the analysis of Y reveals that the most frequent transport occurred in winter, and then followed in fall, spring and summer. This is consistent with the seasonality of the subtropical jet (Koch et al., 2006) and STE in the northern hemisphere, especially results reported for the Tibetan plateau (e.g., Sprenger et al., 2003; Chen et al. 2011; Škerlak et al., 2014), and resembles that of deep stratospheric intrusions over Central Europe (Trickl et al., 2010, 2011). It also shows a similar seasonal cycle with the SI frequency obtained at Mt. Cimone by Cristofanelli et al. (2009) using a SI index, which general idea and structure are similar with the Y indicator. The winter maximum of the

frequency of downward transport corresponds well with the relatively high O_3, relatively low CO and water vapor levels at Xianggelila. Therefore, downward transport of airmasses contributes significantly to the winter level of surface O_3 at Xianggelila. The increase of winter O_3 is estimated to be 21.0 % (+9.6 ppb) due to the impact of deep O_3 transport events.

Acknowledgements

We thank the staff in Diqing Meteorological Bureau for their help during the measurements. This work is supported by Natural Science Foundation of China (21177157, 40830102), and the China Special Fund for Meteorological Research in the Public Interest (GYHY201106023) and Basic Research Fund of CAMS(2011Z003).

References

Bonasoni, P., Evangelisti, F., Bonafe, U., Ravegnani, F., Calzolari, F., Stohl, A., Tositti, L., Tubertini, O., and Colombo, T.: Stratospheric ozone intrusion episodes recorded at Mt. Cimone during the VOTALP project: case studies, Atmos. Environ., 34, 1355-1365, 2000.

Bukin, O. A., An, N. S., Pavlov, A. N., Stolyarchuk, S. Y., Shmirko, K. A.: Effect that Jet Streams Have on the Vertical Ozone Distribution and Characteristics of Tropopause Inversion Layer in the Far East Region, Izvestiya, Atmospheric and Oceanic Physics, 47(5), 610–618, 2011.

Chameides, W., and Walker, J. C. G.: A photochemical theory of tropospheric ozone, J. Geophys. Res., 78, 8751-8760, 1973.

Chen, X. L., Ma, Y. M., Kelder, H., Su, Z., and K. Yang.: On the behaviour of the tropopause folding events over the Tibetan Plateau. Atmos. Chem. Phys., 11, 5113–5122, doi:10.5194/acp-11-5113-2011, 2011.

Chen, X., Anel, J. A., Su, Z., de la Torre, L., Kelder, H., van Peet, J., and Ma, Y.: The deep atmospheric boundary layer and its significance to the stratosphere and troposphere exchange over the Tibetan Plateau, PLOS ONE, 8, e56909, doi:10.1371/journal.pone.0056909, 2013.

Cheng, S. Y., Huang, G. H., Chakma, A., Hao, R. X., Liu L., Zhang, X. H.: Estimation of atmospheric mixing heights using data from airport meteorological stations, Journal of Environmental Science and Health, Part A, 36:4, 521 – 532, 2001.

445 Cooper, O., Moody, J., Parrish, D., Trainer, M., Holloway, J., Hübler, G., Fehsenfeld, F., and Stohl,
446 A.: Trace gas composition of midlatitude cyclones over the western North Atlantic Ocean: A
447 seasonal comparison of O_3 and CO, J. Geophys. Res., 107, 4057, 2002.
448 Cristofanelli, P.,Calzolari, F.,Bonafè, U., Duchi, R., Marinoni, A., Roccato, F., Tositti, L., Bonasoni,
449 P.: Stratospheric intrusion index (SI^2) from baseline measurement data, Theoretical and Applied
450 Climatology, 97, 317-325, 2009.
451 Cristofanelli, P., Braccini, A., Sprenger, M., Marinoni, A., Bonafè, U., Calzolari, F., Duchi, R., Laj,
452 P., Pichon, J., and Roccato, F.: Tropospheric ozone variations at the Nepal Climate
453 Observatory-Pyramid (Himalayas, 5079 m asl) and influence of deep stratospheric intrusion
454 events, Atmos. Chem. Phys., 10, 6537-6549, 2010.
455 Crutzen, P. J.: Photochemical reactions initiated by and influencing ozone in unpolluted tropospheric
456 air, Tellus, 26, 47-57, 1974.
457 Crutzen, P. J., Lawrence, M. G., and Pöschl, U.: On the background photochemistry of tropospheric
458 ozone, Tellus B, 51, 123-146, 1999.
459 Danielsen, E. F.: Stratospheric-tropospheric exchange based on radioactivity, ozone and potential
460 vorticity, Journal of the Atmospheric Sciences, 25, 502-518, 1968.
461 Davies, T., and Schuepbach, E.: Episodes of high ozone concentrations at the earth's surface
462 resulting from transport down from the upper troposphere/lower stratosphere: a review and case
463 studies, Atmos. Environ., 28, 53-68, 1994.
464 Ding A., and Wang T.: Influence of stratosphere-to-troposphere exchange on the seasonal cycle of
465 surface ozone at Mount Waliguan in western China. Geophys. Res.Lett., 33, L03803, doi:
466 10.1029/ 2005GL024760,2006.
467 Draxler, R., and Rolph, G.: HYSPLIT (HYbrid Single-Particle Lagrangian Integrated Trajectory)
468 model access via NOAA ARL READY website (http://www.arl.noaa.gov/ready/hysplit4.html).
469 NOAA Air Resources Laboratory, Silver Spring, Md, 2003.
470 Fishman, J., Solomon, S., and Crutzen, P. J.: Observational and theoretical evidence in support of a
471 significant in‐situ photochemical source of tropospheric ozone, Tellus, 31, 432-446, 1979.
472 Gettelman, A., Kinnison, D. E., Dunkerton, T. J., and Brasseur, G. P.: Impact of monsoon
473 circulations on the upper troposphere and lower stratosphere, J. Geophys. Res., 109, D22101,
474 doi:10.1029/2004JD004878, 2004.

475 Gidel, L. T., and Shapiro, M.: General circulation model estimates of the net vertical flux of ozone in
476 the lower stratosphere and the implications for the tropospheric ozone budget, J. Geophys. Res.,
477 85, 4049-4058, 1980.
478 He, Y., Uno, I., Wang, Z., Pochanart, P., Li, J., and Akimoto, H.: Significant impact of the East Asia
479 monsoon on ozone seasonal behavior in the boundary layer of Eastern China and the west Pacific
480 region, Atmos. Chem. Phys., 8, 7543-7555, 2008.
481 Hough, A. M., and Derwent, R. G.: Changes in the global concentration of tropospheric ozone due to
482 human activities, Nature, 344, 645-648, 1990.
483 Jacob, D. J.: Heterogeneous chemistry and tropospheric ozone, Atmos. Environ., 34, 2131-2159,
484 2000.
485 Jain, S., Arya, B., Kumar, A., Ghude, S. D., and Kulkarni, P.: Observational study of surface ozone
486 at New Delhi, India, International Journal of Remote Sensing, 26, 3515-3524, 2005.
487 Junge, C. E.: Global ozone budget and exchange between stratosphere and troposphere, Tellus, 14,
488 363-377, 1962.
489 Klausen, J., Zellweger, C., Buchmann, B., and Hofer, P.: Uncertainty and bias of surface ozone
490 measurements at selected Global Atmosphere Watch sites, J. Geophys. Res., 108, 4622, 2003.
491 Koch, P., Wernli, H., and Davies, H. C.: An Event-based Jet-stream Climatology and Typology, Int.
492 J. Climatol., 26, 283–301, 2006.
493 Krupa, S. V., and Manning, W. J.: Atmospheric ozone: formation and effects on vegetation, Environ.
494 Pollut., 50, 101-137, 1988.
495 Langford, A. O.: Stratosphere-troposphere exchange at the subtropical jet, contribution to the
496 tropospheric ozone budget at midlatitudes, Geophys. Res. Lett, 26, 2449–2452, 1999.
497 Langford, A. O., OLeary, T. J., Masters, C. D., Aikin, K. C., and Proffitt, M. H.: Modulation of
498 middle and upper tropospheric ozone at Northern midlatitudes by the El Ni˜no/Southern
499 Oscillation, Geophys. Res. Lett., 25, 2667–2670, 1998.
500 Lefohn, A. S., Oltmans, S. J., Dann, T., and Singh, H. B.: Present-day variability of background
501 ozone in the lower troposphere, J. Geophys. Res., 106, 9945-9958, 2001.
502 Liang, M. C., Tang, J., Chan, C. Y., Zheng, X., and Yung, Y. L.: Signature of stratospheric air at the
503 Tibetan Plateau, Geophys. Res. Lett., 35, 2008.

504 Logan, J., Staehelin, J., Megretskaia, I., Cammas, J. P., Thouret, V., Claude, H., De Backer, H.,
505 Steinbacher, M., Scheel, H. E., and Stübi, R.: Changes in ozone over Europe: Analysis of ozone
506 measurements from sondes, regular aircraft (MOZAIC) and alpine surface sites, J. Geophys. Res.,
507 117, D09301, doi:10.1029/2011JD016952., 2012.
508 Ma J., Zheng X D., Xu X D.: Comment on "Why does surface ozone peak in summertime at Wa
509 Liguan?" by Bin Zhu et al., Geophys. Res.Lett., 32: 01805, doi: 00.1029/2004GL0-21683,2005.
510 Ma J., Zhou, X., and Hauglustaine, D.: Summertime tropospheric ozone over China simulated with a
511 regional chemical transport model 2. Source contributions and budget, J. Geophys. Res., 107(D22),
512 4612, doi:10.1029/2001JD001355, 2002..
513 Marenco, A., Thouret, V., Nédélec, P., Smit, H., Helten, M., Kley, D., Karcher, F., Simon, P., Law,
514 K., and Pyle, J.: Measurement of ozone and water vapor by Airbus in-service aircraft: The
515 MOZAIC airborne program, an overview, J. Geophys. Res., 103, 25631-25642, 1998.
516 Monks, P. S.: A review of the observations and origins of the spring ozone maximum, Atmos.
517 Environ., 34, 3545-3561, 2000.
518 Moore, G., and Semple, J. L.: A Tibetan Taylor Cap and a halo of stratospheric ozone over the
519 Himalaya, Geophys. Res. Lett., 32, L21810, 2005.
520 Naja, M., and Lal, S.: Changes in surface ozone amount and its diurnal and seasonal patterns, from
521 1954–55 to 1991–93, measured at Ahmedabad (23 N), India, Geophys. Res. Lett., 23, 81-84,
522 1996.
523 Neuman, J., Trainer, M., Aikin, K., Angevine, W., Brioude, J., Brown, S., de Gouw, J., Dube, W.,
524 Flynn, J., and Graus, M.: Observations of ozone transport from the free troposphere to the Los
525 Angeles basin, J. Geophys. Res., 117, D00V09, 2012.
526 Ordóñez, C., Brunner, D., Staehelin, J., Hadjinicolaou, P., Pyle, J., Jonas, M., Wernli, H., and Prévôt,
527 A.: Strong influence of lowermost stratospheric ozone on lower tropospheric background ozone
528 changes over Europe, Geophys. Res. Lett., 34, L07805, 2007.
529 Oltmans, S., Lefohn, A., Shadwick, D., Harris, J., Scheel, H., Galbally, I., Tarasick, D., Johnson, B.,
530 Brunke, E.-G., and Claude, H.: Recent tropospheric ozone changes–A pattern dominated by slow
531 or no growth, Atmos. Environ., 2012.

Parrish, D., Law, K. S., Staehelin, J., Derwent, R., Cooper, O., Tanimoto, H., Volz-Thomas, A., Gilge, S., Scheel, H.-E., and Steinbacher, M.: Long-term changes in lower tropospheric baseline ozone concentrations at northern mid-latitudes, Atmos. Chem. Phys., 12, 11485-11504, 2012.

Randel, W. J., Seidel, D. J., and Pan, L. L.: Observational characteristics of double tropopauses, J. Geophys. Res., 112, D07309, doi:10.1029/2006JD007904, 2007

Rolph, G.: Real-time Environmental Applications and Display sYstem (READY) Website (http://ready.arl.noaa.gov). NOAA Air Resources Laboratory, Silver Spring, MD, USA, 2010.

Skamarock, W. C., Klemp, J. B., Dudhia, J., Gill, D. O., Barker, D. M., Wang, W., and Powers, J. G.: A description of the Advanced Research WRF Version 2, DTIC Document, 2005.

Škerlak, B., Sprenger, M., and Wernli, H.: A global climatology of stratosphere–troposphere exchange using the ERA-Interim data set from 1979 to 2011, Atmos. Chem. Phys., 14, 913-937, doi:10.5194/acp-14-913-2014, 2014.

Sprenger, M., and Wernli, H.: A northern hemispheric climatology of cross-tropopause exchange for the ERA15 time period (1979–1993), J. Geophys. Res., 108, 8521, 2003.

Sprenger, M., Maspoli, M. C., and Wernli, H.: Tropopause folds and cross-tropopause exchange: A global investigation based upon ECMWF analyses for the time period March 2000 to February 2001, J. Geophys. Res., 108, 8518, 2003.

Staehelin, J., Harris, N., Appenzeller, C., and Eberhard, J.: Ozone trends: A review, Reviews of Geophysics, 39, 231-290, 2001.

Stohl, A., and Trickl, T.: A textbook example of long-range transport- Simultaneous observation of ozone maxima of stratospheric and North American origin in the free troposphere over Europe, J. Geophys. Res., 104, 445-462, 1999.

Stohl, A., Spichtinger-Rakowsky, N., Bonasoni, P., Feldmann, H., Memmesheimer, M., Scheel, H., Trickl, T., Hübener, S., Ringer, W., and Mandl, M.: The influence of stratospheric intrusions on alpine ozone concentrations, Atmos. Environ., 34, 1323-1354, 2000.

Tang J., Wen Y., Xu X., Zheng X., Guo S., and Zhao Y.: China global atmosphere watch baseline observatory and its measurement program, CAMS Annual Report 1994-1995, China Meteorology Press, Beijing, 56-65, 1995.

Tilmes, S., Pan, L. L., Hoor, P., Atlas, E., Avery, M. A., Campos, T., Christensen, L. E., Diskin, G. S., Gao, R.- S., Herman, R. L., Hintsa, E. J., Loewenstein, M., Lopez, J., Paige, M. E., Pittman, J.

562 V., Podolske, J. R., Proffitt, M. R., Sachse, G. W., Schiller, C., Schlager, H., Smith, J., Spelten, N.,
563 Webster, C., Weinheimer, A., and Zondlo M. A.: An aircraft-based upper troposphere lower
564 stratosphere O_3, CO, and H_2O climatology for the Northern Hemisphere, J. Geophys. Res., 115,
565 D14303, doi:10.1029/2009JD012731, 2010.
566 Trickl, T., Bärtsch-Ritter, N., Eisele, H., Furger, M., Mücke, R., Sprenger, M., and Stohl, A.:
567 High-ozone layers in the middle and upper troposphere above Central Europe: potential import
568 from the stratosphere along the subtropical jet stream, Atmos. Chem. Phys., 11, 9343-9366,
569 doi:10.5194/acp-11-9343-2011, 2011.
570 Trickl, T., Feldmann, H., Kanter, H.-J., Scheel, H.-E., Sprenger, M., Stohl, A., and Wernli, H.:
571 Forecasted deep stratospheric intrusions over Central Europe: case studies and climatologies,
572 Atmos. Chem. Phys., 10, 499-524, 2010.
573 Vaughan, G., and Price, J.: On the relation between total ozone and meteorology, Q. J. Royal
574 Meteorol. Soc., 117, 1281-1298, 1991.
575 Vingarzan, R.: A review of surface ozone background levels and trends, Atmos. Environ., 38,
576 3431-3442, 2004.
577 Wang, T., Wong, H., Tang, J., Ding, A., Wu, W., and Zhang, X.: On the origin of surface ozone and
578 reactive nitrogen observed at a remote mountain site in the northeastern Qinghai-Tibetan Plateau,
579 western China, J. Geophys. Res., 111, D08303, 2006.
580 Wang, Z. and Sassen, K.: Ozone destruction in continental stratus clouds: An aircraft case study，J.
581 Appl. Meteorol. 39(6): 875-886, 2000.
582 Xu X., Tang, J., and Lin, W.: The trend and variability of surface ozone at the global GAW station
583 Mt. WALIGUAN, China, in “Second Tropospheric Ozone Workshop Tropospheric Ozone
584 Changes: Observations, state of understanding and model performances”, WMO/GAW report,
585 WMO, Geneva, 49-55, 2011.
586 Xue, L. K., Wang, T., Zhang, J. M., Zhang, X. C., Deliger, Poon, C. N., Ding, A. J., Zhou, X. H.,
587 Wu, W. S., Tang, J., Zhang, Q. Z., and Wang, W. X.: Source of surface ozone and reactive
588 nitrogen speciation at Mount Waliguan in western China: New insights from the 2006 summer
589 study, J. Geophys. Res., 116, D07306, doi:10.1029/2010JD014735, 2011.

590 Zheng X., Shen C., Wan G., Liu K., Tang J., and Xu X.: $^{10}Be/^{7}Be$ implies the contribution of
591 stratosphere -troposphere transport to the winter-spring surface O_3 variation observed on the
592 Tibetan Plateau, Chinese Science Bulletin, 56: 84−88, 2011.
593 Zheng X., Wan G., Tang J., Zhang X., Yang W., Lee H., and Wang C.: ^{7}Be and ^{210}Pb radioactivity
594 and implications on sources of surface ozone at Mt. Waliguan, Chinese Science Bulletin, 50(2):
595 167-171, 2005.

Table 1. Monthly mean O_3 and CO, the average diurnal O_3 maxima, minima, and amplitudes

Month	O_3[ppbv]				CO[ppbv]
	Mean±SD	Diurnal Max(local time)	Diurnal Min(local time)	Diurnal amplitude	Mean±SD
JAN	45.4±5.6	49.2(14:00)	41.4(8:00)	7.9	139±56
FEB	50.6±5.8	54.3(12:00)	47.2(8:00)	7.1	153±46
MAR	57.1±6.9	61.4(12:00)	50.5(8:00)	10.8	185±57
APR	58.3±8.8	63.7(13:00)	50.1(7:00)	13.6	182±59
MAY	50.2±9.8	58.4(13:00)	39.9(7:00)	18.5	181±54
JUN	37.4±11.6	46.6(13:00)	27.9(6:00)	18.7	146±40
JUL	26.8±12.5	34.8(13:00)	18.5(7:00)	16.3	153±47
AUG	24.2±8.8	31.8(13:00)	17.3(6:00)	14.5	156±42
SEP	29.6±9.2	37.7(13:00)	20.3(6:00)	17.4	159±41
OTC	31.4±10.1	37.5(14:00)	24.1(8:00)	13.4	124±36
NOV	38.1±7.8	42.8(14:00)	33.1(9:00)	9.7	118±44
DEC	39.7±5.0	44.7(14:00)	36.1(10:00)	8.6	119±53

Table 2. Average air temperature (^{o}C), wind speed (m/s), specific humidity (g/kg), O_3 and CO volume mixing ratios (ppb) associated with different types of trajectories and seasonal fractioning of trajectories.

Type	T	Wind speed	humidity	O_3	CO	Spring(%)	Summer(%)	Fall(%)	Winter(%)
1	-1.9	2.8	1.5	53.5	99	50.0	0.0	0.0	50.0
2	5.0	1.8	5.0	43.8	126	38.6	18.6	17.1	25.7
3	1.6	2.1	2.1	40.5	93	4.0	0.0	28.0	68.0
4	0.9	1.9	2.4	36.0	98	10.2	0.7	21.1	68.0
5	3.2	2.3	4.2	44.8	139	46.8	2.2	17.4	33.6
6	7.1	1.9	7.9	32.6	135	17.1	37.4	28.3	17.3
7	9.5	1.6	9.7	27.6	150	14.6	49.5	35.8	0.0

Table 3. Numbers of hours and consecutive days meeting the different Y criteria

		Y>3	Y>4	Y>5	Y>6	Y>7	Y>8
numbers of hours		784	396	218	138	88	72
numbers of consecutive days	ALL	200	136	91	63	46	38
	Spring	42	23	15	10	5	4
	Summer	32	14	11	9	5	4
	Fall	58	43	29	19	16	12
	Winter	65	53	32	21	17	15

Table 4. Monthly results of the O_3–CO correlation, derived from 10:00–18:00 (local time) measurements from Xianggelila. The slopes and intercepts of the regression lines were derived using the reduced-major-axis regression technique.

Month	intercept	slope	R^2	P	N
JAN	33.5	0.109	0.0007	0.59	392
FEB	35.9	0.117	0.0494	<0.0001	438
MAR	38.7	0.119	0.1950	<0.0001	521
APR	39.7	0.136	0.1160	<0.0001	519
MAY	83.4	-0.192	0.0531	<0.0001	509
JUN	85.2	-0.344	0.0861	<0.0001	516
JUL	-14.0	0.347	0.0540	<0.0001	497
AUG	-3.1	0.233	0.0411	<0.0001	515
SEP	67.5	-0.251	0.0547	<0.0001	461
OTC	65.2	-0.285	0.1080	<0.0001	499
NOV	58.4	-0.183	0.0693	<0.0001	420
DEC	50.7	-0.094	0.0551	0.02	300

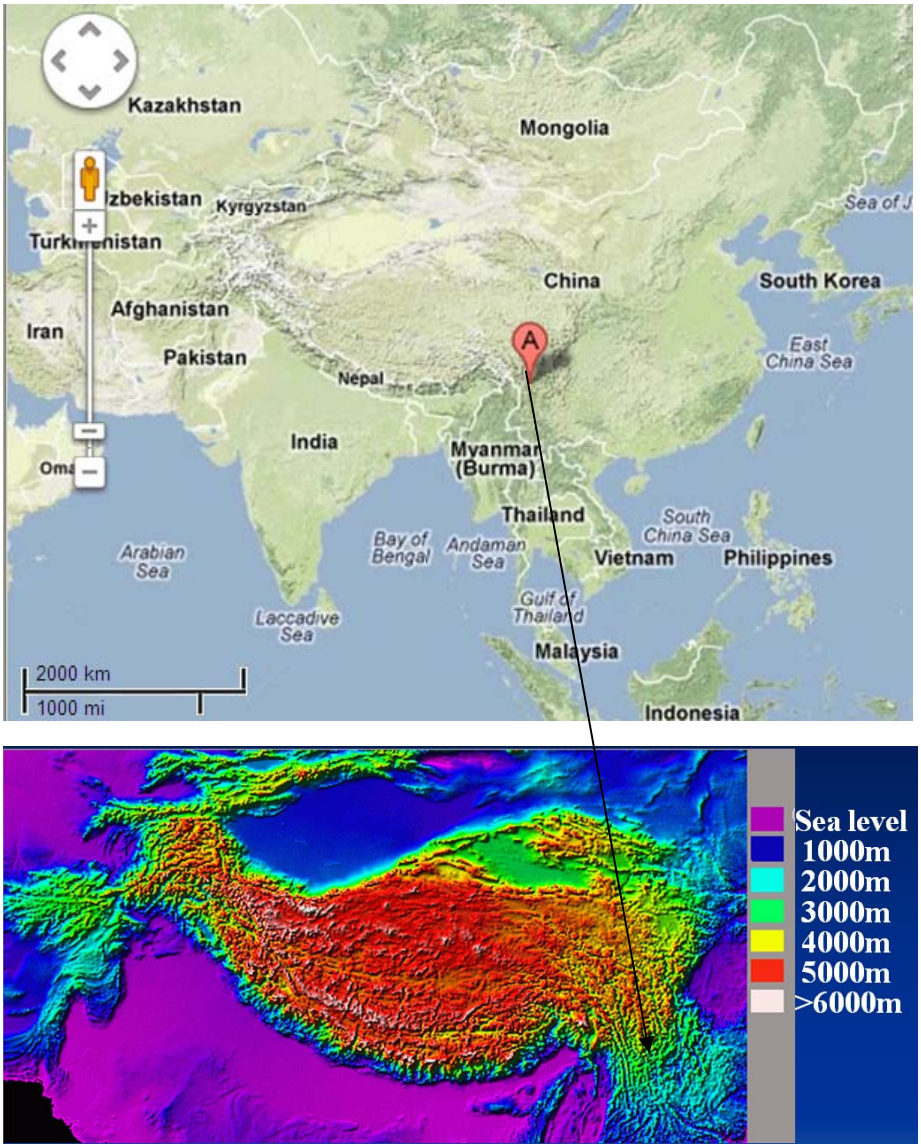

Fig .1 The geographical location of the Xianggelila Regional Atmosphere Background Station (the upper is from Google map and the bottom is from NASA earth).

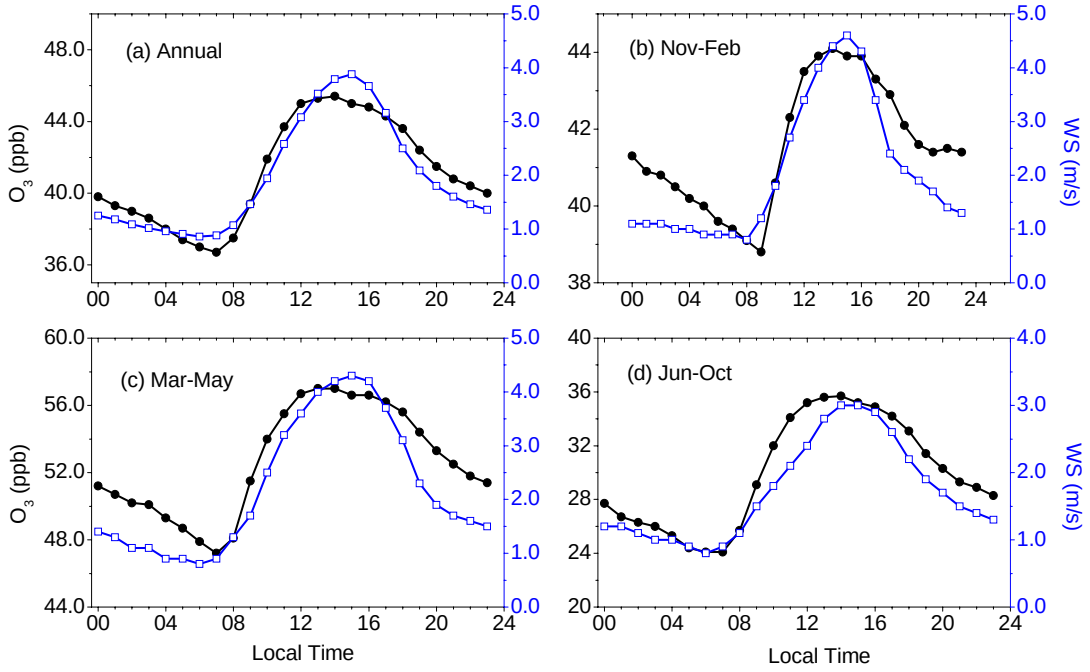

Fig 2. The average diurnal variations of O_3 and wind speed (WS) at the Xianggelila station for different periods.

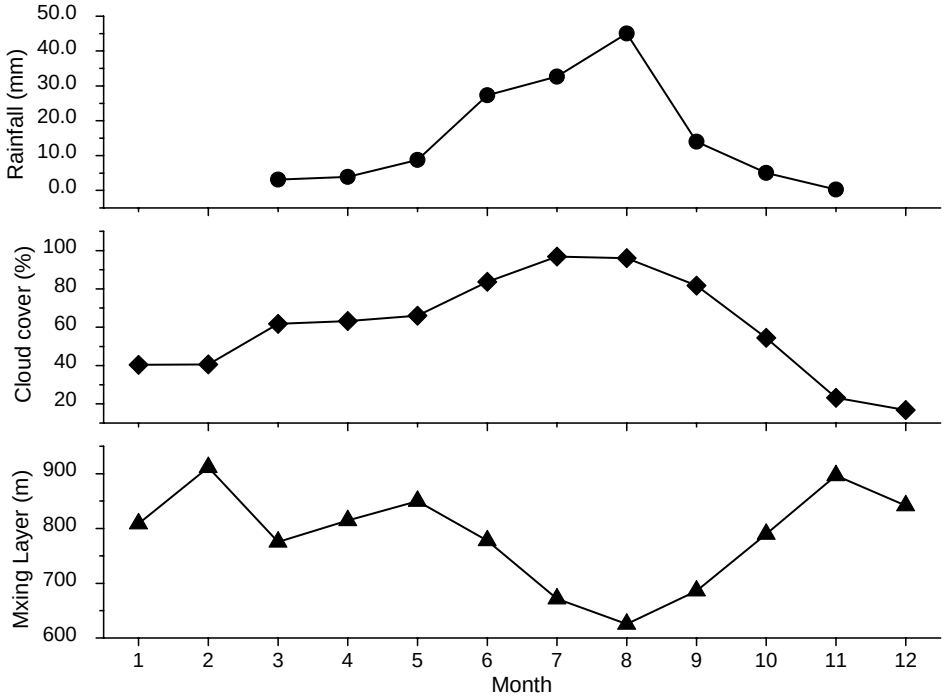

Fig. 3 Monthly variations of rainfall, cloud cover and boundary mixing layer height at Xianggelila station.

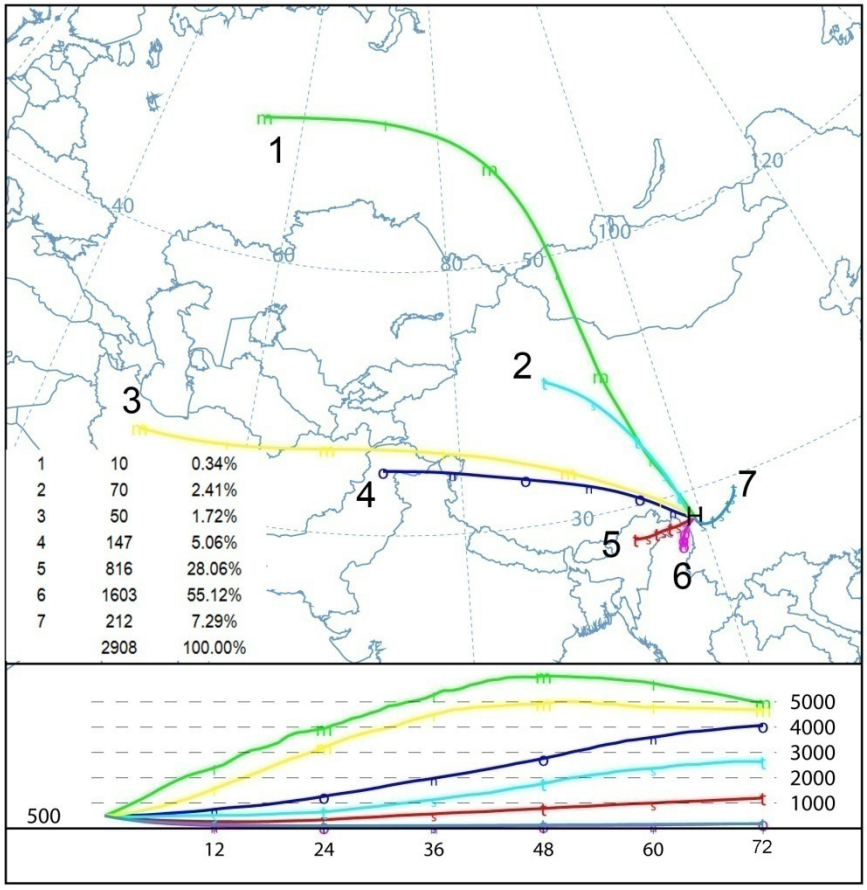

Fig. 4 Mean backward trajectories ending at Xianggelila. The endpoint height is 500 m a.g.l. The numbers of trajectories in each cluster and their percent ratios among the total trajectories are shown. The unit of trajectory height is m a.g.l.

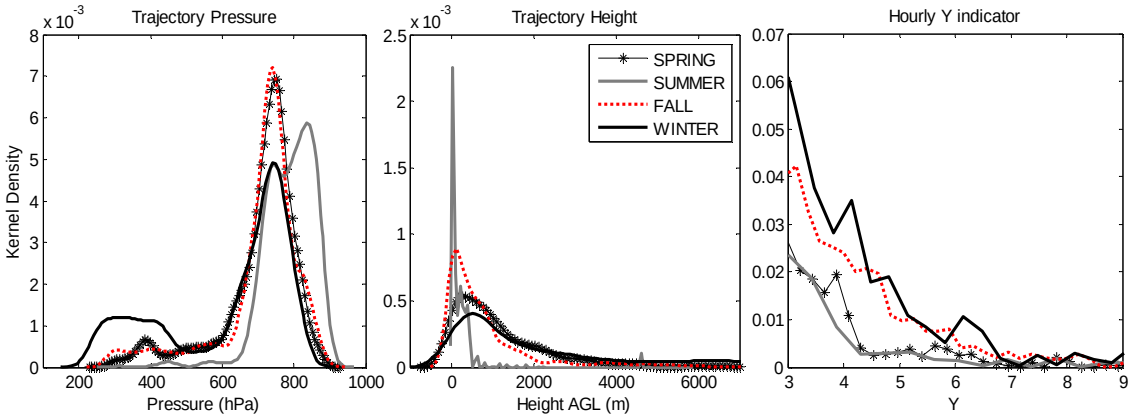

Fig. 5 Kernel probability density of trajectory pressure level, trajectory height above ground level and hourly Y indicator in each season.

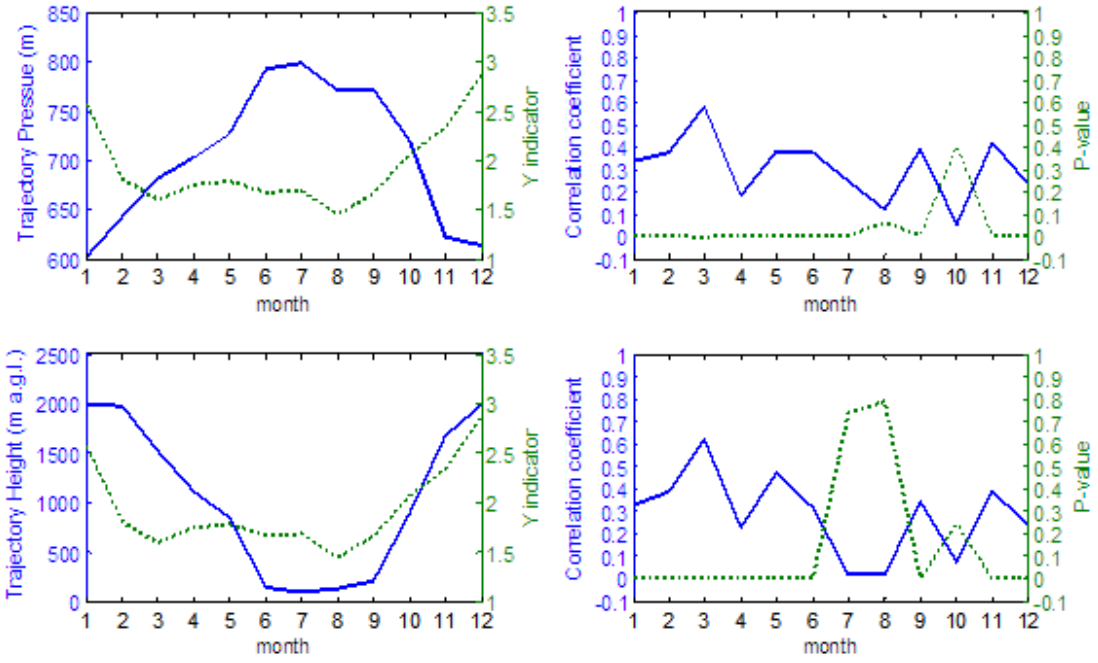

Fig. 6 Correlation between trajectory pressure level or height and Y indicator with significant levels (P-value). The upper-left graph shows monthly trends of trajectory pressure and Y indicator, while the upper-right is the correlation between both. The lower-left graph shows monthly trends of trajectory height and Y indicator, while the lower-right is the correlation between both. Note that correlation between trajectory pressure and Y indicator is actually negative, but shown in absolute value.

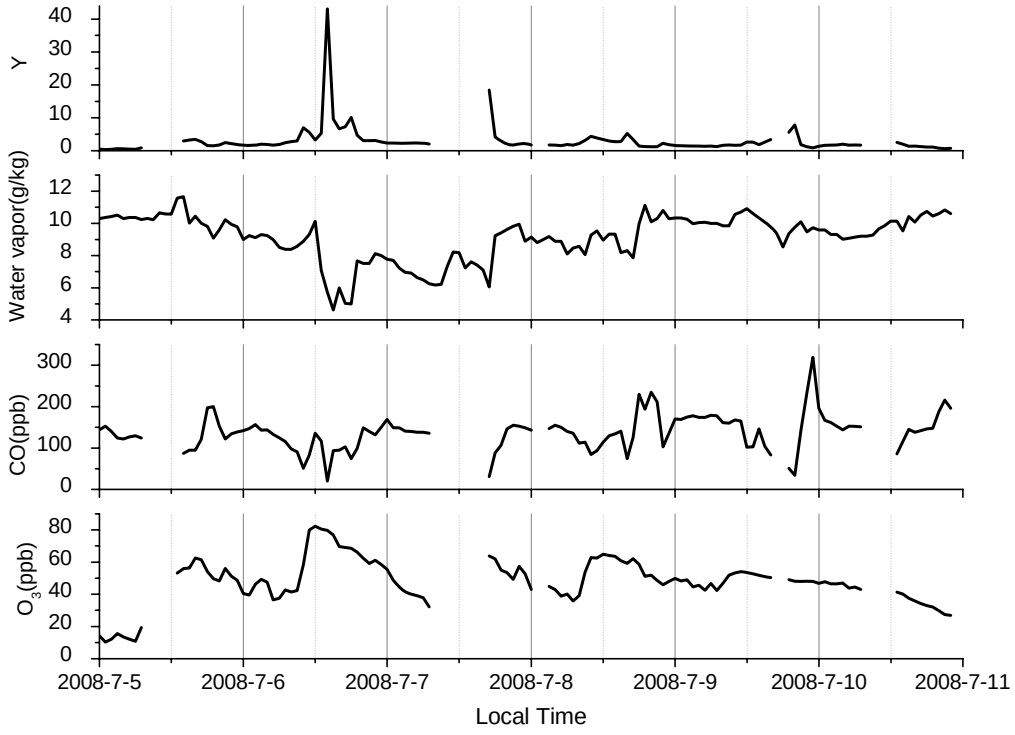

Fig. 7 Time series of Y value, water vapor, CO and O_3 mixing ratios from July 5 to July 11, 2008.

596

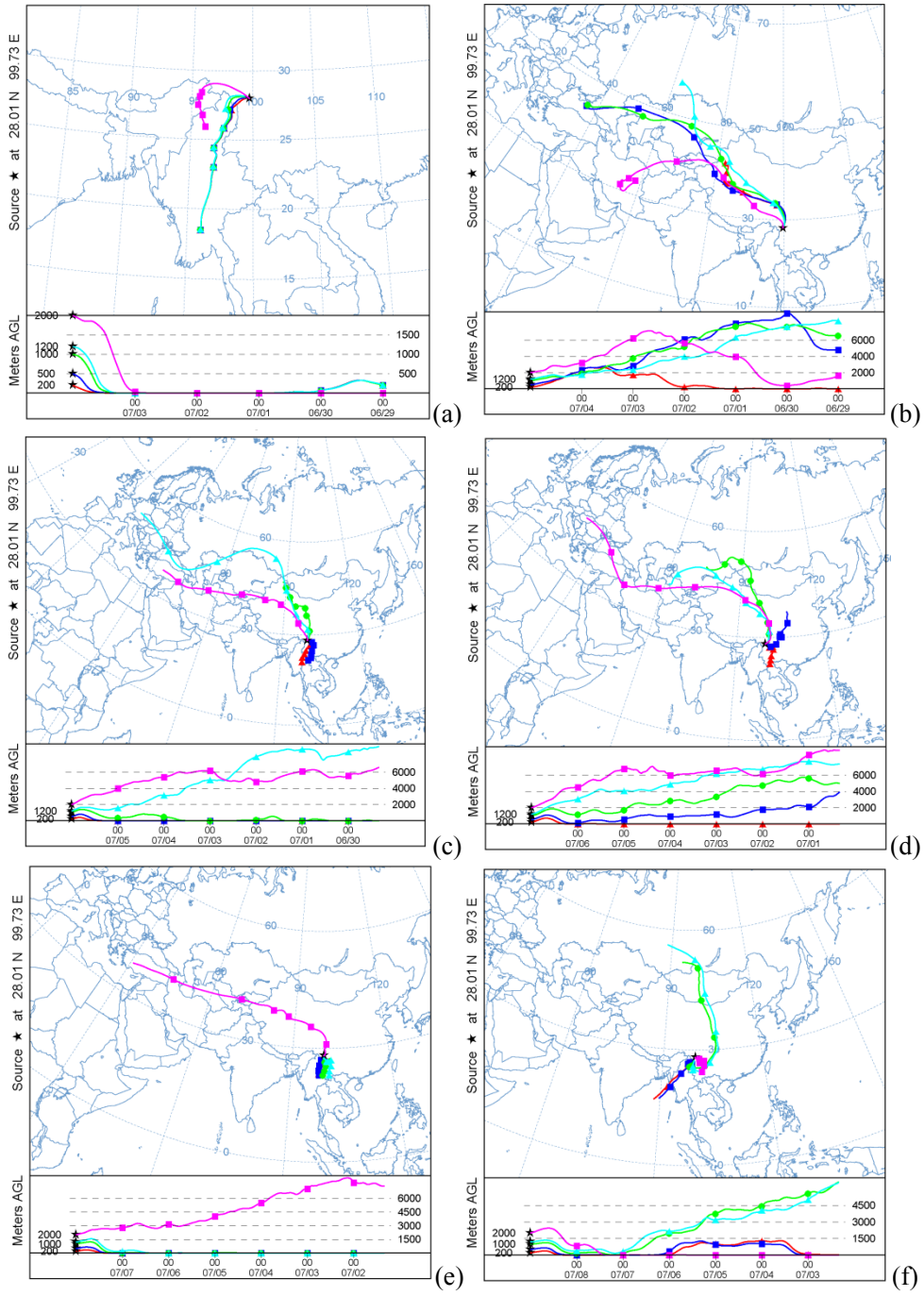

Fig. 8 Seven-day backward trajectories arriving at different heights over Xianggelila from 4 July to 9 July 2008. Backward trajectories ending at 0000 UTC on July 04 (a), July 05 (b), July 06(c), July 07(d), July 08 (e), and July 09(f).

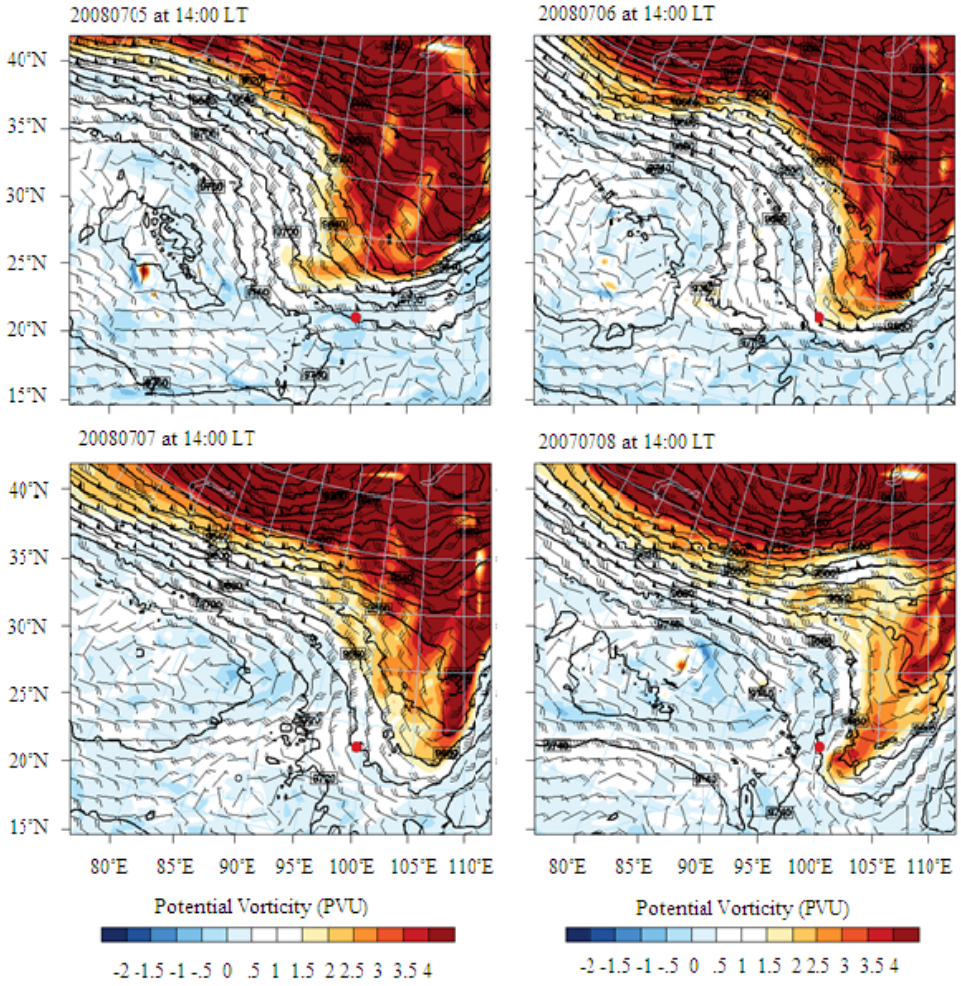

Fig. 9 Geopotential height, horizontal wind vector on 300 hPa and potential vorticity on 350 K from July 5 to July 8, 2008. The filled red circle denotes the Xianggelila station.

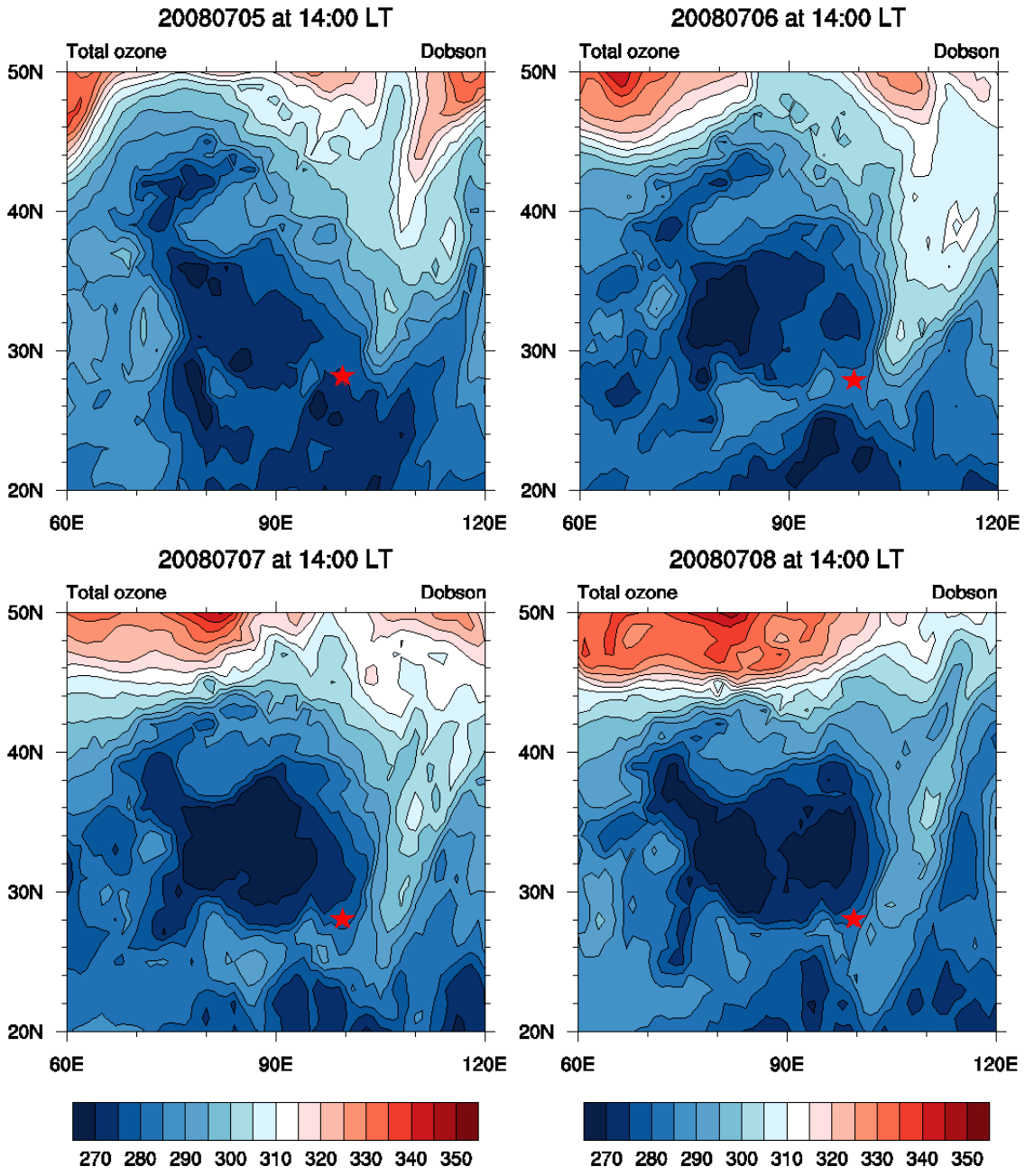

Fig. 10 Total column O_3 from July 5 to July 8 2008. The red pentacle denotes the Xianggelila station.

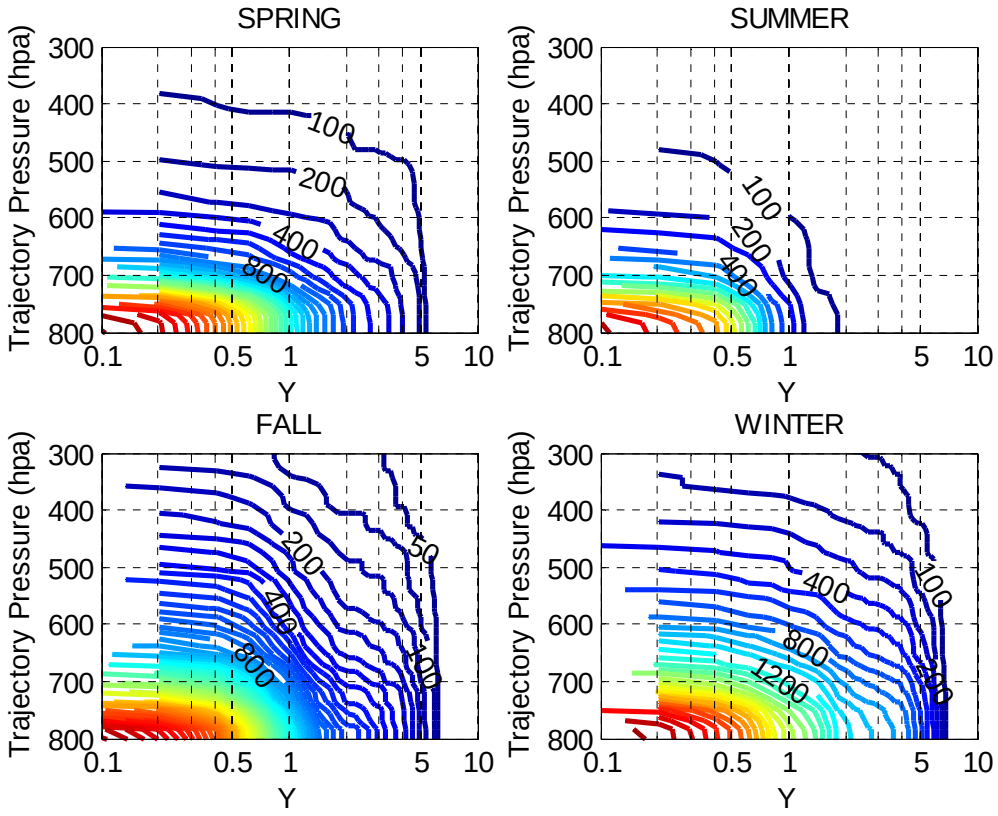

Fig. 11 Hours with both trajectory pressure lower than and Y value larger than given values in different seasons. Note that X-axis is in logarithmic coordinate.

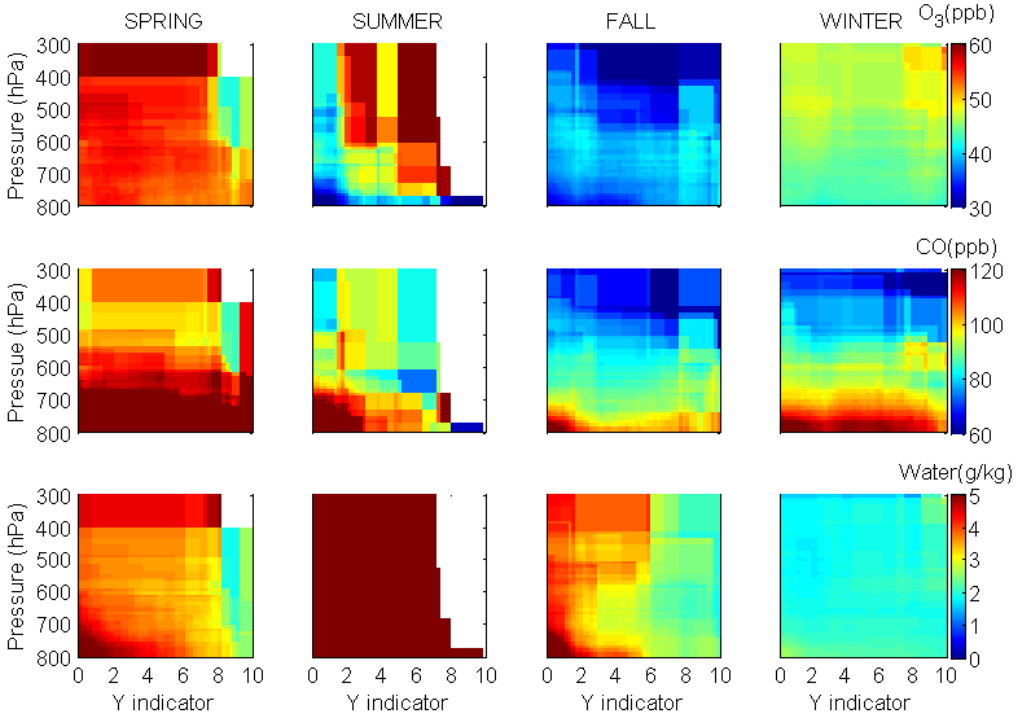

Fig. 12 Distributions of the values of O_3, CO, and water vapor above specific trajectory pressure levels and the values of Y indicator. Y-axis denotes trajectory pressure (hPa) and X-axis denotes Y indicator. Units of color bar of O_3 and CO are ppb; of water vapor is g/kg.